



Ellipsometry-based conductivity extraction in case of phosphorus doped polysilicon

A. Kemiha¹ · B. Birouk¹ · J.-P. Raskin²

Received: 17 January 2018 / Accepted: 8 May 2018 / Published online: 17 May 2018
© Springer Science+Business Media, LLC, part of Springer Nature 2018

Abstract

In this work, we investigated a new method for thin films electrical conductivity extraction based on spectroscopic ellipsometry. This has been enabled through the correlation between the films conductivity and their ellipsometric properties. Indeed, it has been demonstrated that numerous ellipsometric fitting-based approaches can provide, in an indirect way, the electrical characteristics of thin films. The study was focused on electrical conductivity, but doping level or carriers' mobility can also be extrapolated from ellipsometric measurements. Among various possibilities leading to electrical properties extraction, we can cite the extremal values of Ψ and Δ ellipsometric angles, their associated wavelengths, the mean square error and the maximal and minimal reflectivities ratio. Otherwise, the correlation between extrinsic conductivity and ellipsometric parameters evolution has been confirmed in case of low doping levels with particular behavior after annealing. This contactless method has been successfully applied to polycrystalline silicon films deposited on oxidized, p-type monocrystalline substrates, by low pressure chemical vapor deposition technique, and lightly or heavily phosphorus doped by diffusion. The feasibility of the method has been proven in this case, but also in other cases like implanted polysilicon layers or silicon-on-insulator (not included here).

1 Introduction

Spectroscopic ellipsometry is a powerful technique considered as one of the most routinely used ones worldwide in laboratories and cleanrooms, mainly in thin films optical characterization case. But when researchers study ellipsometric technique and electrical conductivity, the aim is to characterize the thin films from separated optical and electrical points of view. These properties result especially in the case of physical constants determination from the spectral or electrical responses of these films toward an excitation. Many optical devices are used to perform optical measurements, and in quite all cases, theoretical or semi-empirical

methods support the analyses, which must take into account the main electrical and physical characteristics of the layers. Among the influencing parameters, we can mention doping level (carriers' concentration), deposition temperature and layer thickness (grain size), surface quality (roughness), and so on. Ellipsometry which is an accurate, non-destructive and contactless technique based on beam light reflection analysis is frequently used for extracting layer's characteristics as thickness, refractive index, extinction coefficient and roughness [1–5]. In this work, the resulting experimental angles Ψ and Δ were studied and fitted in relation with doping level and layer thickness, in order to get access to morphological and optical parameters. As demonstrated hereafter the electrical conductivity of polycrystalline silicon layer can be extracted with pretty good accuracy by using a variety of graphical methods from Ψ and Δ curves.

Polycrystalline silicon (shortened to polysilicon) has been widely studied and used throughout the world, with the main aim to substitute the monocrystalline silicon. The deposition and characterization of the polysilicon layers are carried out by using various techniques. low pressure chemical vapor deposition (LPCVD) technique is massively used due to the relative low deposition temperature, added to excellent uniformity, good step coverage, and superior cost

✉ B. Birouk
bbirouk@univ-jijel.dz

A. Kemiha
adel_kemiha@yahoo.fr

J.-P. Raskin
jean-pierre.raskin@uclouvain.be

¹ Renewable Energies Laboratory (LER), Jijel University, Jijel, Algeria

² ICTEAM, Université catholique de Louvain (UCL), Louvain-la-Neuve, Belgium

effectiveness [6] of the produced layers. Many important applications have been implemented in microelectronics and photovoltaic areas. Among these, we can find load resistors, CMOS gates, interconnections in integrated circuits, diffusion source, active layer in solar cells, and in MEMS. It is known that the deposition conditions influence greatly the polysilicon properties and that these films are completely crystallized for deposition temperature above 600 °C [3, 7]. The layers surface is characterized by relatively great roughness when they are thick enough or grown at high deposition temperature [3, 8].

2 Samples and characterization setups

To perform this study, we used two series of $1.5 \times 1.5 \text{ cm}^2$ polycrystalline silicon samples: the first series is based on high phosphorus doping level, while the second one is lightly doped and has been annealed. The substrate is p-type, CZ <100> oriented, with $381 \mu\text{m}$ ($\pm 20 \mu\text{m}$) thickness and lightly doped (resistivity of between 10 and 20 Ωcm). The c-Si substrates were thermally oxidized during 2 h and 28 min, under temperature of 1000 °C, to obtain oxide thickness of around 100 nm. The undoped polysilicon layers were deposited in LPCVD furnace (40 sccm of SiH_4), at temperature of 620 °C, resulting in thickness of 175 and 100 nm for S and E-series, respectively. The doping process was carried out after standard cleaning, by phosphorus diffusion from phosphorus pentoxide glass source. To achieve heavily n-type doping, six wafers of the S-series have been submitted to high temperature about 900 °C, for various periods of diffusion time: 15, 20, 25, 30, 35 and 45 min, followed by glass etching. The same procedure was followed for the four doped samples of the second series (denoted E), with diffusion time of 3, 5, 8, 25 min. The samples surface and cross section images have been taken with a scanning electron microscope (SEM) of Ultra 55 model, while for atomic force microscopy (AFM) ones we used Peak Force Tapping with PPP NCHR tip.

The optical and morphological characteristics of our deposited films have been typically determined by means of a Gaerdner type Spectroscopic Ellipsometer (SE) of SENTECH Instruments. The investigation has been performed by using six layers structure model: air, native oxide, roughness, polysilicon, thermal oxide, c-Si substrate (Fig. 1). The incident angle Φ of the light beam was initially set at 70°. A Cauchy layer model was used to compute the optical parameters in the visible–near infrared (Vis–NIR) spectral range. The total error during SE fitting sessions was lowered to its minimum by reducing the partial errors on which one can act, like fixed values (beam incidence angle, oxide and polysilicon thicknesses, effective medium approximation (EMA) roughness, etc), misalignment of the angle of incidence [9], bad software

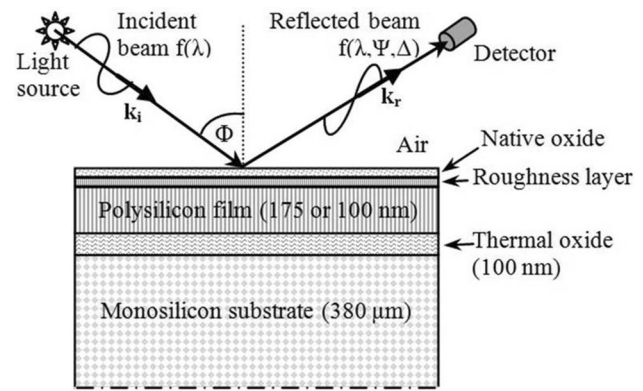


Fig. 1 Structure model used in Ellipsometry showing incident and reflected beams (transmitted one is not represented)

convergence (operator–software interaction), specific measuring error (operator–ellipsometer interaction), and so on. Electrical characterization was based on conductivity measurements by means of a HMS 3000 type Hall Effect device.

3 Optical model

Ellipsometry characterization is a non-destructive technique based on the analysis of the parallel and perpendicular components of the reflected light beam. It allows the knowledge of several optical parameters, in addition to thickness and roughness. These parameters define well the optical behavior of the studied layers. One can cite among these, the reflectance $R(\lambda)$ and transmittance $T(\lambda)$, the Ψ and Δ ellipsometric angles, the refractive $n(\lambda)$ and extinction $k(\lambda)$ coefficients, the absorption $\alpha(\lambda)$ and optical band gap E_g , for the major ones.

The fundamental relation of the Ellipsometry gives the complex Fresnel reflection coefficient ratio ρ as in Eq. (1):

$$\tilde{\rho} = \frac{\tilde{R}^p}{\tilde{R}^s} = \tan \Psi \exp(i\Delta) \quad (1)$$

where coefficients R^p and R^s characterize the reflection of parallel and perpendicular wave components, respectively, and are given in case of 3 layers system by

$$\tilde{R}^p = \frac{\tilde{r}_{12}^p + \tilde{r}_{23}^p \exp(-2i\tilde{\beta})}{1 + \tilde{r}_{12}^p \tilde{r}_{23}^p \exp(-2i\tilde{\beta})} \quad (2)$$

$$\tilde{R}^s = \frac{\tilde{r}_{12}^s + \tilde{r}_{23}^s \exp(-2i\tilde{\beta})}{1 + \tilde{r}_{12}^s \tilde{r}_{23}^s \exp(-2i\tilde{\beta})} \quad (2')$$

The polarization state analysis of the reflected light by means of the Ψ and Δ ellipsometric angles leads then to optical characterization of the layers.

The ratios $\tilde{r}_{ij}^p(\tilde{r}_{ij}^s)$ is the complex reflection coefficients for p-polarized (s-polarized) waves, and the complex coefficient $\tilde{\beta}$ is linked to thickness d , complex refractive index $\tilde{N} = n - ik$, and incidence angle φ by the following expression:

$$\tilde{\beta} = 2\pi \left(\frac{d}{\lambda}\right) \tilde{N} \cos \varphi \tag{3}$$

On the other hand, the Drude model allows us to express the complex permittivity of a dielectric middle of conductivity σ , when crossed by radiation of pulsation ω , as follows [10]:

$$\tilde{\epsilon}_{(\omega)} = \tilde{N}^2 = \tilde{\epsilon} + \frac{-1 + i/\tau\omega}{1 + \omega^2\tau^2} \frac{\sigma\tau}{\epsilon_0} \tag{4}$$

where $\tau = \mu m^*/q$ and $\sigma = n\mu q$, are relaxation time and extrinsic conductivity of the layer, and m^* , q , μ and n are free carriers effective mass, elementary charge, mobility and concentration, respectively.

These four equations give the evidence that the ellipsometric angles are linked to the electrical conductivity of the layers and consequently will vary when the doping level will change.

Besides, we have to take into consideration the practical characteristics (layer type, thickness, doping type and level, roughness, etc.) of the active layers to model well their optical behavior, knowing that this latter is strongly depending on experimental conditions.

4 Experimental results

To point out the structural characteristics of the layers used in this study and correlate them with ellipsometric measurements, cross-section and top surface SEM images as well as AFM measurements of the samples top surface have been performed.

One notices in Figs. 2 and 3, the particular shape of the crystallites which looks like grenadine grains one, with roughness peaks up to 25 nm. The shape greatly columnar is characterized by five neighbors having interface two by two, and showing on the surface a non-regular pentagonal shape.

The manual estimation of the crystallites size in Fig. 4a–g, leads to the results collected in Table 1. It appears clearly that the heavy phosphorus doping influence in an undoubted way the grains growth (20–70% larger, relatively to undoped sample), and besides, the final size is all greater as the doping level is higher (mainly for very high doping concentration). It may be noted that several processes occur during diffusion doping, e.g. annealing, crystallite growth and activation of free carriers [11, 12].

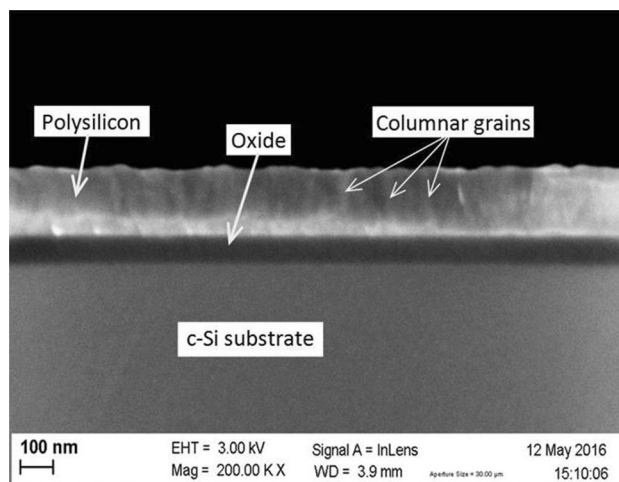


Fig. 2 SEM cross-section of the S-series structures

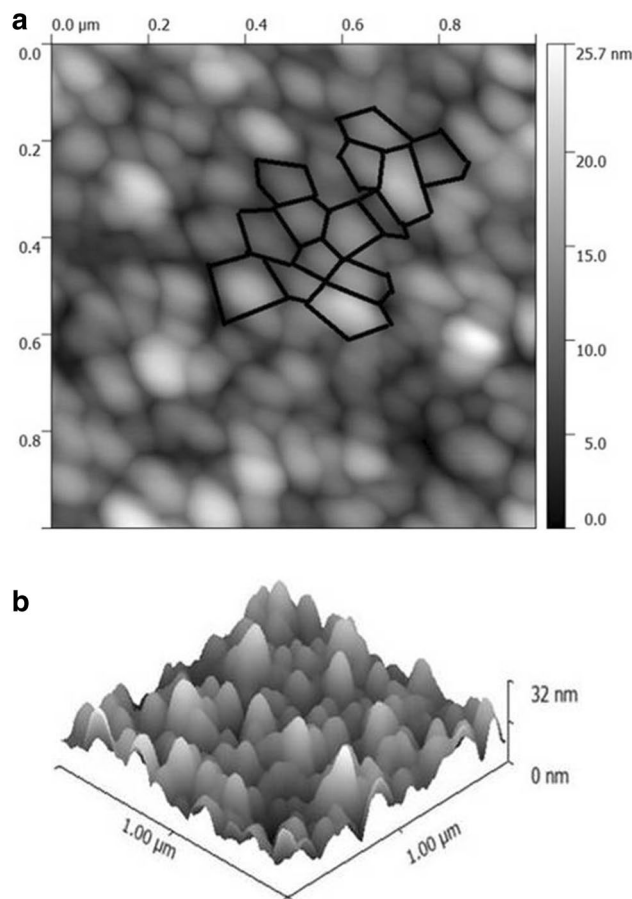


Fig. 3 a 1 × 1 μm² AFM image of S-series doped polysilicon films, with some examples of non-regular pentagons. b 3D AFM image of S-series doped polysilicon films

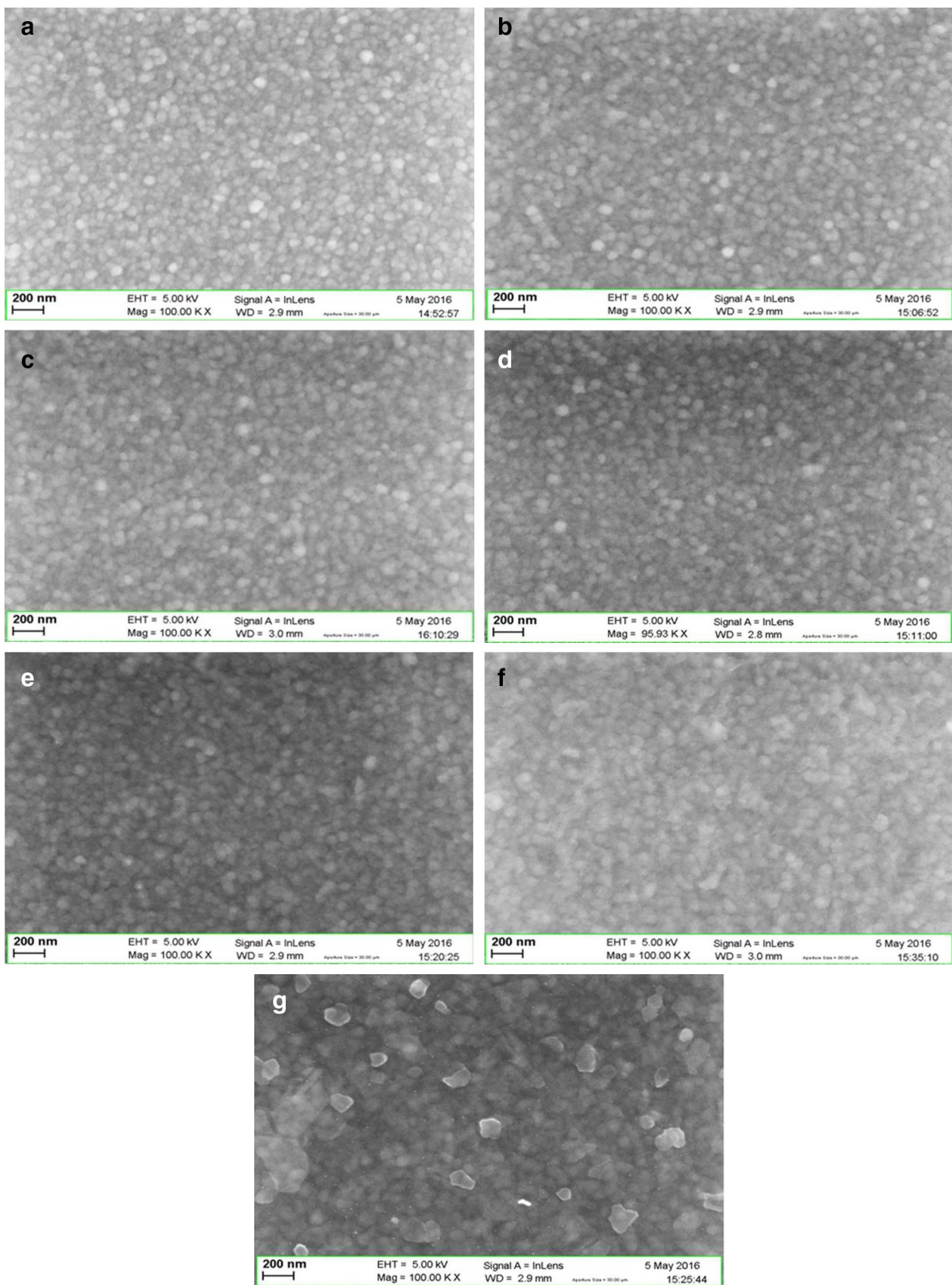


Fig. 4 SEM images of the S-series polysilicon films according to phosphorus doping level. **a:** Undoped, **b:** $5.5 \times 10^{19} \text{ cm}^{-3}$, **c:** $7.6 \times 10^{19} \text{ cm}^{-3}$, **d:** $9.1 \times 10^{19} \text{ cm}^{-3}$, **e:** $1.09 \times 10^{20} \text{ cm}^{-3}$, **f:** $1.41 \times 10^{20} \text{ cm}^{-3}$, **g:** $1.88 \times 10^{20} \text{ cm}^{-3}$

Table 1 Crystallites size estimation of polysilicon layers

Sample	Phosphorus concentration (cm ⁻³)	Average grains number over image length	Grain size estimation (nm)
S1	Undoped	40	76
S2	5.5 × 10 ¹⁹	33	93
S3	7.6 × 10 ¹⁹	34	
S4	9.1 × 10 ¹⁹	35	
S5	1.09 × 10 ²⁰	34	
S6	1.41 × 10 ²⁰	29	106
S7	1.88 × 10 ²⁰	24	128

At this stage of the study, one can call attention to S7 sample, which is very highly phosphorus doped, and whose surface is characterized by some protruding crystallites, with size between of 120 and 200 nm, added to many other nanocrystallites or clusters of diameter around 10 nm, distributed on the surface. This latter is rougher than the other samples surface.

SEM/AFM characterizations show that the polysilicon layers are meanly rough. The Ellipsometry-based study allowed us to appreciate the layers roughness with mean values found about 22 Å for the undoped film, and between of 23 and 58 Å, for the doped ones. This result is in agreement with what has been published elsewhere in the literature [12, 13] in case of similar deposition conditions.

The polysilicon reflectance analysis, by means of ellipsometry, required the implementation of a 6-layer structure model, composed of c-Si substrate, oxide, polysilicon, native oxide layer and an EMA roughness layer based on linear growth of air medium.

In Figs. 5 and 6, the variations of the ellipsometric angles Ψ and Δ as function of radiation wavelength are plotted. The main characteristics highlighted on these curves are the extrema values Ψ_{max}, Ψ_{min}, Δ_{max1}, Δ_{max2}, the wavelengths associated to them and the gap between them. In another work [14], the same applied experimental conditions (LPCVD, 620 °C, <100>-oriented oxidized-substrate, incident angle 70°) lead to similar curves but with a second minimum over the same spectral range, owing to a thicker polysilicon layer (250 nm). The gap δλ = λ_{Ψmax} - λ_{Ψmin}, in this case is lower, about 120 nm instead of 160 nm for our film thickness (175 nm).

The radiation passes through the polysilicon film and reaches the polysilicon/oxide interface where it is reflected, to get out again and meet at infinity the light reflected on polysilicon surface, where they interfere constructively or destructively together. One can remark that both of these states are associated to maximal or minimal intensity reflected, in other words to reflectivity extrema values, hence Ψ extrema values are directly related to

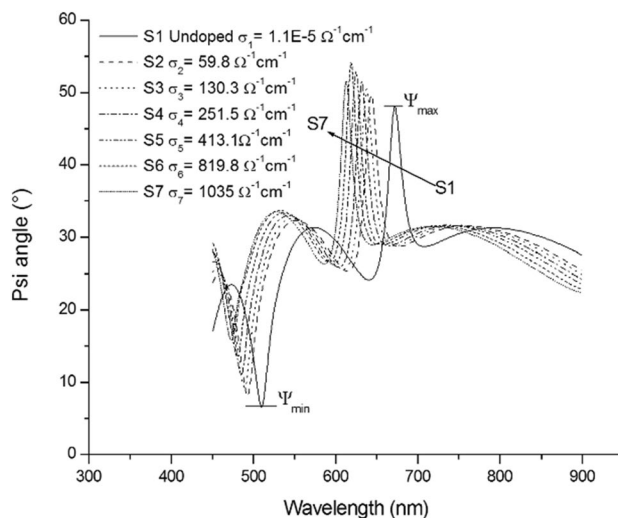


Fig. 5 Ψ angle values before and after phosphorus doping versus wavelength, for S-series structures

layer thickness *d* and refractive index *n*, by the following relationships:

$$2 n(\lambda_{\Psi_{max}}) d = m \lambda_{\Psi_{max}} \tag{5}$$

$$2 n(\lambda_{\Psi_{min}}) d = (m + 1/2) \lambda_{\Psi_{min}} \tag{6}$$

where λ_{Ψmax}, λ_{Ψmin}, n(λ_{Ψmax}), n(λ_{Ψmin}) and *d* are ellipsometry results and *m* is the interference order.

As noticed in Figs. 5 and 6, ellipsometric angles curves are regularly shifted towards lower wavelengths when the electrical conductivity increases. Moreover, the wavelengths gap δλ between the extrema angles, for the same curve, is monotonically decreasing in the same situation.

The analysis of Fig. 5 emphasizes the fact that Ψ angle maxima and minima increase with the doping level, until

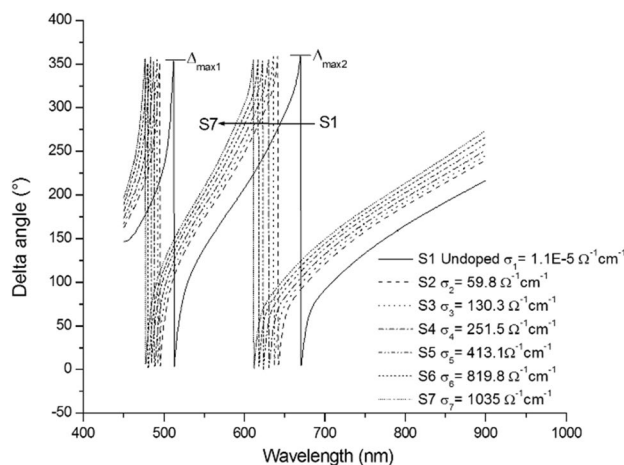


Fig. 6 Δ angle values before and after phosphorus doping versus wavelength for S-series structures

the phosphorus concentration approaches (or exceeds) the degeneracy limit, then started to diminish. On the other hand, the Δ angle extrema remain approximately constant as we can see in Fig. 6.

Figure 7 represents the variations of Ψ maxima and minima as a function of the polysilicon layer conductivity logarithm, which is translated into the following relationships (valid for σ below 900 S/cm):

$$\Psi_{\min} = -8.54 + 3.71 \times \text{Ln}(\sigma) \text{ and } \Psi_{\max} = 41.3 + 1.899 \times \text{Ln}(\sigma) \tag{7}$$

This allows us to determine σ (and ρ) knowing just one of the Ψ extrema values. It may be noted at this level, that this method gives an estimation of the conductivity and is not an accurate measurement of this latter. The uncertainties are less than 20% in the majority of the cases (see Table 2), when the ellipsometry and conductivity measurements are made with a minimum error. We think that this contactless method is suitable for layer quality monitoring in an industrial fabrication chain by applying the following procedure:

1. For calibration purpose the conductivity of at least two samples is measured by another technique;

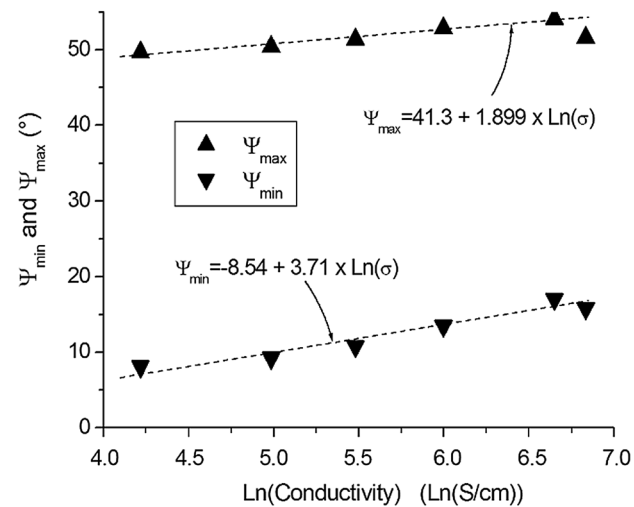


Fig. 7 Ψ angle extrema values evolution versus polysilicon layer conductivity logarithm for S-series structures

2. One extracts their Ψ_{\max} (or Ψ_{\min}) from ellipsometric measurements;
3. One draws the 2 points $(\sigma_1, \Psi_{\max1})$ and $(\sigma_2, \Psi_{\max2})$ on an xy plan, and connecting them with a straight line;
4. Now, measuring the Ψ_{\max} value of a third sample allows deducting its conductivity by reporting the measured value on the plan.

Even if these calculus methods are not a straightforward manner to extract the extrinsic conductivity, they remain a good way to avoid electrical contacts on surface and destruction of the samples, mainly in case of small areas. We can extend the procedure to other deposition procedure, and establish a nomogram for different experimental conditions.

The evolution of Δ and Ψ curves (shift and extrema values variation) can be related to two main influent sources. In the first place, the evolution of the free electrons concentration modifies the complex refractive index in accordance to Drude theory (correlation between spectroscopic ellipsometry and conductivity measurements). Secondly, the polysilicon layer crystallinity and roughness increase with the doping level, following the thermal budget during the diffusion process [12].

Now, if we take into account the wavelengths associated to Ψ and Δ extrema values, we get the linear profiles appearing in Fig. 8.

These profiles lead to extrinsic conductivity determination (up to 900 S/cm) by using one of the following expressions:

$$\begin{aligned} &\exp\left(\frac{686 - \lambda_{\Psi_{\max}}}{9.88}\right) \text{ or } \exp\left(\frac{686 - \lambda_{\Delta_{\max2}}}{10.45}\right) \text{ or} \\ &\exp\left(\frac{521 - \lambda_{\Delta_{\max1}}}{6.26}\right) \text{ or } \exp\left(\frac{521 - \lambda_{\Psi_{\min}}}{6.77}\right) \end{aligned} \tag{8}$$

One can see in Table 3 that the layers conductivity calculated by this method approaches its measured value with accuracy lesser than 20 in 90% of the cases.

One can remark obviously that the difference between the wavelengths, $\delta\lambda = \lambda_{\Psi_{\max}} - \lambda_{\Psi_{\min}}$ or $\lambda_{\Delta_{\max2}} - \lambda_{\Delta_{\max1}}$, will give rise to equivalent profiles and relationships, if plotted as function of conductivity.

Table 2 Comparison between measured and calculated polysilicon layers conductivity, for “ Ψ method”

Sample	σ_{meas} (S/cm)	Ψ_{\max} method		Ψ_{\min} method	
		σ_{cal} (S/cm)	Relative error (%)	σ_{cal} (S/cm)	Relative error (%)
S2	59.8	88.9	48.7	83.4	39.4
S3	130.3	120.9	-7.2	120.5	-7.5
S4	251.5	183.6	-27.0	204.1	-18.8
S5	413.1	380.2	-8.0	449.7	8.8
S6	819.8	976.6	19.1	845.9	3.2

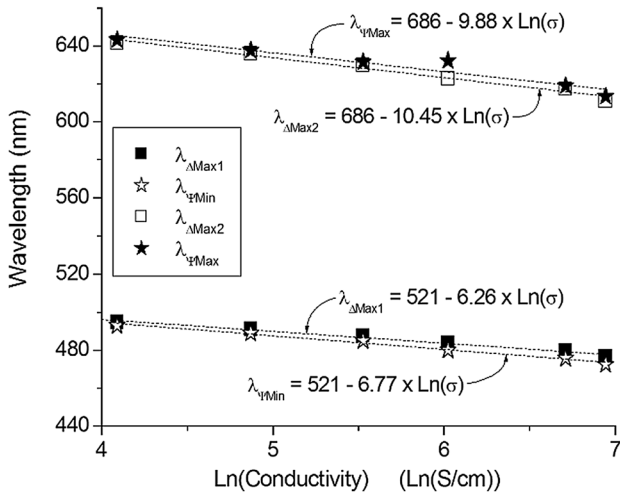


Fig. 8 Wavelengths associated to Ψ and Δ angles extrema values as function of polysilicon layer conductivity logarithm for S-series structures

Furthermore, we considered two experimental Ψ curves; the first plotted before phosphorus diffusion and the second after, and determined the mean squared error (MSE) [14] with a modified formulation as follows:

$$MSE_{Si} = \frac{1}{2N - p} \sum_{j=1}^N \left[\left(\Psi_{(\lambda_j) \text{exp}}^{Si} - \Psi_{(\lambda_j) \text{exp}}^{S1} \right)^2 + \left(\Delta_{(\lambda_j) \text{exp}}^{Si} - \Delta_{(\lambda_j) \text{exp}}^{S1} \right)^2 \right] \quad (9)$$

where Si refers to sample i ($i = 2$ to 7), N the number of data points ($N = 561$) and p the variable parameters number ($p = 19$). The results are reported in Fig. 9 where the linear increase of the MSE with conductivity enhancement (in logarithmic scale) is observed.

From Fig. 9, one can determine the conductivity of polysilicon layer by comparing its ellipsometric angles curves with the undoped samples, and applying the relationship (10):

$$\sigma = \exp \left(\frac{\text{Ln}(MSE) - 2.436}{0.1825} \right) \quad (10)$$

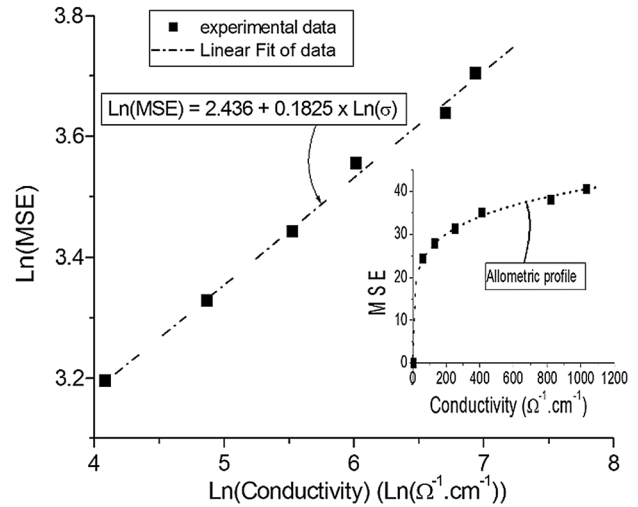


Fig. 9 Evolution of MSE (Eq. 9) versus conductivity, in log–log scale for S-series structures (linear scale for the inset)

The “MSE method” is apparently more accurate than the two previous ones (relative error below 12% as shown in Table 4), and moreover allows us to perform accurate extraction for conductivity exceeding 1000 S/cm.

The extrinsic conductivity of the deposited films can also be determined by another method which we named the “reflectance ratio method”. Figure 10 visualizes the evolution of the ratio between of maxima and minima values of the reflectance ratio amplitude $\rho = \tan \Psi$ with conductivity variation. The figure clearly shows an exponential decay profile that is used to deduce conductivities up to 1100 S/cm and more with good accuracy (see Table 5), by applying the following relationship:

$$\sigma = 441.3 - 268 \text{Ln} \left(\frac{\tan \Psi_{Max}}{\tan \Psi_{Min}} - 4.34 \right) \quad (11)$$

After this study, we added another series, denoted E (see Table 6), with diffusion time less than for S-series, to have lower phosphorus doping level, in order to corroborate the results issued from the first series and point out

Table 3 Comparison between measured and calculated polysilicon layers conductivity for “wavelength method”

Sample	σ_{meas} (S/cm)	$\lambda_{\Psi_{\text{max}}}$ method		$\lambda_{\Psi_{\text{min}}}$ method		$\lambda_{\Delta_{\text{max1}}}$ method		$\lambda_{\Delta_{\text{max2}}}$ method	
		σ_{cal} (S/cm)	Relative error (%)	σ_{cal} (S/cm)	Relative error (%)	σ_{cal} (S/cm)	Relative error (%)	σ_{cal} (S/cm)	Relative error (%)
S2	59.8	66.77	11.6	62.55	4.6	70.02	17.1	76.09	27.2
S3	130.3	120.58	−7.5	112.93	−13.3	119.66	−8.2	132.78	1.9
S4	251.5	207.57	−17.5	203.89	−18.9	214.52	−14.7	248.69	−1.1
S5	413.1	393.25	−4.8	426.72	3.3	423.20	2.4	231.68	−43.9
S6	819.8	733.22	−10.6	805.36	−1.8	709.52	−13.5	890.25	8.6

Table 4 Comparison between measured and calculated polysilicon layers conductivity for “MSE method”

Method	Sample	Measured value (S/cm)	Calculated value (S/cm)	Relative error (%)
MSE	S2	59.8	63.9	6.9
	S3	130.3	132.4	1.6
	S4	251.5	247.6	-1.6
	S5	413.1	459.7	11.3
	S6	819.8	727.0	-11.3
	S7	1035	1038.8	0.4

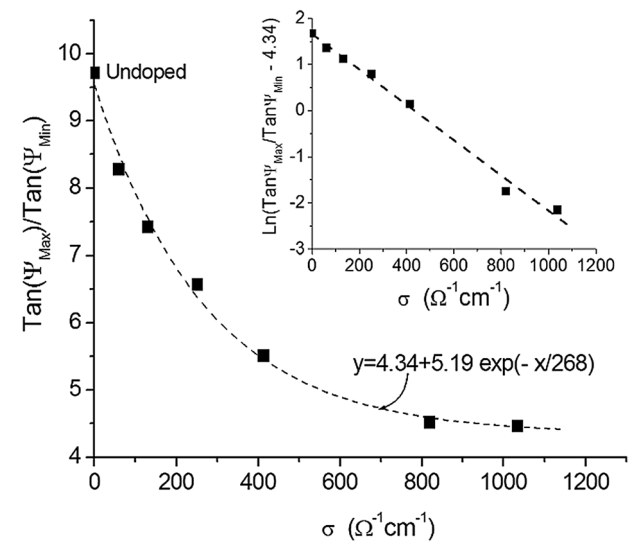


Fig. 10 Evolution of the reflectivities ratio ρ_{max}/ρ_{min} (see Eq. 1) versus conductivity for S-series structures

Table 5 Comparison between measured and calculated polysilicon layers conductivity for reflectance ratio method

Method	Sample	Measured value (S/cm)	Calculated value (S/cm)	Relative error (%)
$\frac{\tan\Psi_{Max}}{\tan\Psi_{Min}}$	S2	59.8	74.4	24.4
	S3	130.3	139.9	7.3
	S4	251.5	227.1	-9.7
	S5	413.1	400.4	-3.1
	S6	819.8	906.3	10.6
	S7	1035	1016.5	-1.8

the annealing effect. Ψ angle variation versus wavelength, after doping and annealing, is reported in Fig. 11.

One can remark in Fig. 11, that the Ψ maxima and minima fall on the same wavelengths ranges for the doped samples of both series. It can be seen also, that the layer reflectivity has been increased after annealing, mainly at maximal values. Furthermore, this figure highlights the great shift of

Table 6 Characteristics of the S- and E-series LPCVD polysilicon films

Sample	$d_{(Polysilicon)}/d_{(oxide)}$ thicknesses (nm)	Diffusion time t_d (min)	Hall Effect Conductivity σ (S/cm)
S1	175/100	Undoped	1.10×10^{-5}
S2		15	59.8
S3		20	130.3
S4		25	251.5
S5		30	413.1
S6		35	819.8
S7		45	1035.0
E1	100/100	Undoped	1.85×10^{-5}
E2	(Annealed at	3	7.4
E3	1000 °C during	5	29.4
E4	60 min)	8	87.1
E5		25	698.6

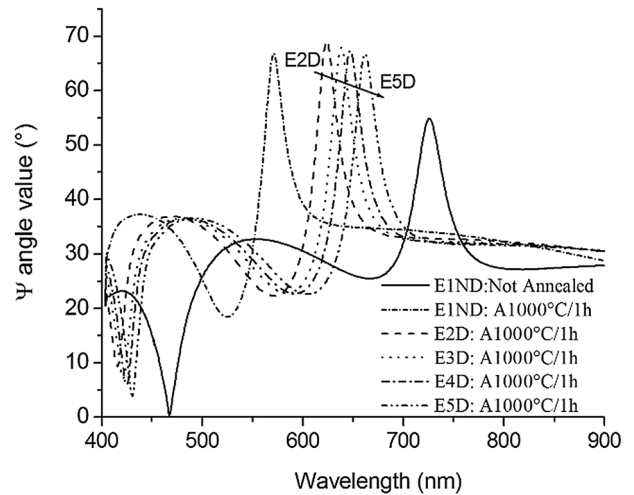


Fig. 11 Ψ angle values versus wavelength, for E-series after annealing at 1000 °C during 1 h, compared with non-annealed undoped layer one

the undoped layer curve towards the small wavelengths, after annealing process. For the doped layers, this shift is smaller as the doping level is larger. Moreover, after the annealing, the reflectivity maxima values and associated wavelengths have undergone variation in the opposite direction of the S-series one: decreasing for the first and increasing for the second. This behavior is emphasized in Figs. 12 and 13, when compared with Figs. 7 and 8.

Ψ variations curve shift and reflectivity maxima values evolution are explained schematically in Fig. 14. Both phenomena might be related to the combined effect of annealing and phosphorus concentration on grain growth, phosphorus

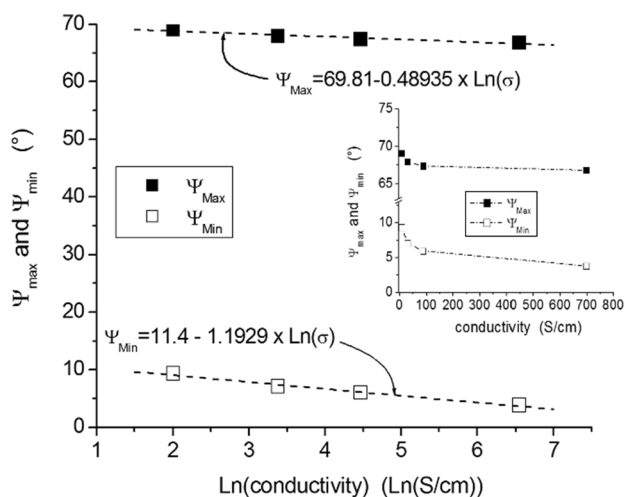


Fig. 12 Ψ angle extremal values evolution versus polysilicon layer conductivity logarithm, for E-series structures

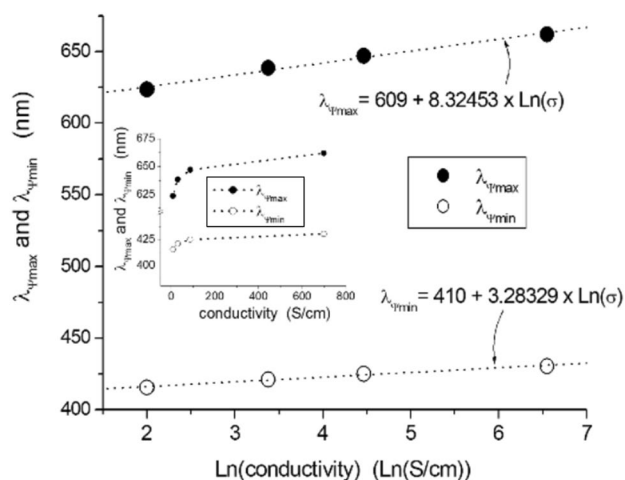


Fig. 13 Wavelengths associated to Ψ angles extremal values of E-series structures versus polysilicon layer conductivity logarithm

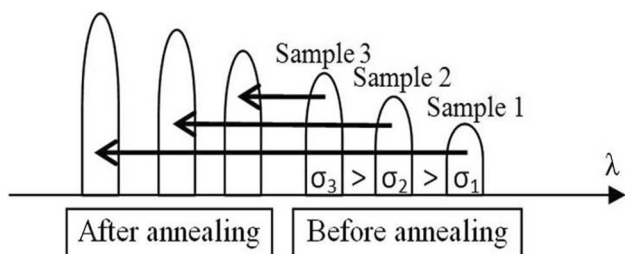


Fig. 14 Explicative schema showing how annealing process acts on Ψ angle peak in low doping level case

distribution and silicon oxidation at the polysilicon/oxide interface.

The linear variations of the Ψ angle extrema values and associated wavelengths, as function of polysilicon layer

conductivity logarithm, allow us to determine σ with a relatively good accuracy, as follows:

$$\sigma = \exp(142.64 - 2.044\Psi_{\max}) \text{ or } \sigma = \exp(9.557 - 0.838\Psi_{\min}) \tag{12}$$

$$\sigma = \exp(0.12\lambda_{\Psi_{\max}} - 73.153) \text{ or } \sigma = \exp(0.305\lambda_{\Psi_{\min}} - 124.87) \tag{13}$$

This study after annealing demonstrates that ellipsometry based conductivity extraction method remains valid even after annealing treatment.

5 Conclusion

In this study, we showed how to use ellipsometry technique to deduct electrical conductivity of thin films, by implementing several methods. The latter have been successfully applied to LPCVD polysilicon layers grown at 620 °C and doped by phosphorus diffusion at 900 °C as example of thin films.

Before that, we studied the structural properties of the films by means of SEM and AFM. Pictures highlighted the crystallites particular shape on the polysilicon layers cross-section (greatly columnar, having interface with five neighbors), and on the surface (non-regular pentagonal shape). The surface roughness is of average value.

We demonstrated that many methods can be applied to extrinsic conductivity estimation based on the complex Fresnel reflection coefficient ratio $\tilde{\rho}$ by implementing the maxima and minima values of the arctan ρ or of the arg ρ . The Ψ and Δ optical parameters representing the ellipsometric measurements give a simple way to get to layer conductivity, in a series developed in the same process. Among these extraction methodologies, the most interesting ones in light of their accuracy are:

- MSE (the most accurate method: average precision about 6%);
- The ratio between of the reflectance ratio amplitude maximal and minimal values $\left(\frac{\tan\Psi_{\max}}{\tan\Psi_{\min}}\right)$;
- Wavelengths associated to Ψ and Δ extrema values ($\lambda_{\Psi_{\max}}$, $\lambda_{\Psi_{\min}}$ and $\lambda_{\Delta_{\max}}$);
- Gap between the latter ($\lambda_{\Psi_{\max}} - \lambda_{\Psi_{\min}}$ and $\lambda_{\Delta_{\max 2}} - \lambda_{\Delta_{\max 1}}$);
- ρ or Ψ extrema values (ρ_{\max} and ρ_{\min} or Ψ_{\max} and Ψ_{\min}).

Acknowledgements We thank very much Mrs Ester Tooten and Mr. Christian Renaux of ICTEAM-UCL, for the preparation of the samples in the clean room facilities named WINFAB.

References

1. X. Li, L. Li, Z. Ma, J. Lu, A.A. Volinsky, F. Ren, Boron doping effects on microcrystalline silicon film roughness studied by spectroscopic Ellipsom. *J. Alloy. Compd.* **684**, 582–586 (2016)
2. B. Birouk, D. Madi, Thermal oxidation effect on structural and optical properties of heavily doped phosphorus polycrystalline silicon films. *Appl. Phys. A* **104**(2), 739–748 (2011). <https://doi.org/10.1007/s00339-011-6332-1>
3. A. Borghesi, G. Tallarida, G. Amore et al., Influence of roughness and grain dimension on the optical functions of polycrystalline silicon films. *Thin Solid Films* **313–314**, 243–247 (1998)
4. M. Modreanu, N. Tomozeiu, M. Gartner, P. Cosmin, Microstructural and optical properties of as-deposited LPCVD silicon films. *Thin Solid Films* **383**, 254–257 (2001)
5. S.A. Memchout, Y. Bouizem, J.D. Sib, A. Belfedal, A. Kebab, D. Benlakehal, L. Chahed, K. Zellama, Effects of ion bombardment on the structural and optical properties in hydrogenated silicon thin films. *Thin Solid Films* **594**, 138–146 (2015)
6. T.W. Ng, T.W. Teo, P. Rajendra, Optical surface roughness evaluation of phosphorus-doped polysilicon. *Opt. Lasers Eng.* **35**, 1–9 (2001)
7. M. Boukezzata, B. Birouk, F. Mandour, D. Bielle-Daspét, Structural and electrical changes in polycrystalline silicon thin films that are heavily in situ boron-doped and thermally oxidized with dry oxygen. *Chem. Vap. Depos.* **3**(N°5), 271–279 (1997)
8. M. Modreanu, M. Gartner, C. Cobianu, B. O’Looney, F. Murphy, Optical properties of silicon thin films related to LPCVD growth condition. *Thin Solid Films* **450**, 105–110 (2004)
9. H. Reisinger, Minimization of errors in ellipsometric measurements. *Solid State Electron.* **35**(3), 333–344 (1992)
10. https://lns.epfl.ch/files/content/sites/lns2/files/lectures/solid/cours/Chapitre_1.pdf. Accessed 09 April 2018
11. L. Asinovsky, M. Schroth, F. Shen, J.J. Sweeney, Characterization and metrology of the diffusion doped polysilicon using Ellipsometry. *Thin Solid Films* **313–314**, 248–253 (1998)
12. H. Günther, *Optical Properties of Polycrystalline Silicon Films*, vol. 57 (Springer Series in Solid-State Sciences, New York, 1985), pp. 156–169
13. P. Petrik, L.P. Biro, M. Fried, T. Lohner, R. Berger, C. Schneider, J. Gyulai, H. Ryssel, Comparative study of surface roughness measured on polysilicon using spectroscopic ellipsometry and atomic force microscopy. *Thin Solid Films* **315**, 186–191 (1998)
14. B. Gruska, Ellipsometric analysis of polysilicon layers. *Thin Solid Films* **364**, 138–143 (2000)